LAWRENCE
LIVERMORE
NATIONAL
LABORATORY

LLNL-PROC-461691

Comparing the use of 4.6 um lasers versus 10.6 um lasers for mitigating damage site growth on fused silica surfaces

S. T. Yang, M. J. Matthews, S. Elhadj, D. Cooke, G. M. Guss, V. G. Draggoo, P. J. Wegner

November 4, 2010

SPIE Laser Damage Conference
Boulder, CO, United States
September 26, 2010 through September 29, 2010

Disclaimer

This work performed under the auspices of the U.S. Department of Energy by Lawrence Livermore National Laboratory under Contract DE-AC52-07NA27344.

Comparing the use of 4.6 μm lasers versus 10.6 μm lasers for mitigating damage site growth on fused silica surfaces

Steven T. Yang*, Manyalibo J. Matthews, Selim Elhadj, Diane Cooke, Gabriel M. Guss, Vaughn G. Draggoo, and Paul J. Wegner
Lawrence Livermore National Laboratory, Livermore, CA 94550

ABSTRACT

The advantage of using mid-infrared (IR) 4.6 μm lasers, versus far-infrared 10.6 μm lasers, for mitigating damage growth on fused silica is investigated. In contrast to fused silica's high absorption at 10.6 μm, silica absorption at 4.6 μm is two orders of magnitude less. The much reduced absorption at 4.6 μm enables deep heat penetration into fused silica when it is heated using the mid-IR laser, which in turn leads to more effective mitigation of damage sites with deep cracks. The advantage of using mid-IR versus far-IR laser for damage growth mitigation under non-evaporative condition is quantified by defining a figure of merit (FOM) that relates the crack healing depth to laser power required. Based on our FOM, we show that for damage cracks up to at least 500 μm in depth, mitigation using a 4.6 μm mid-IR laser is more efficient than mitigation using a 10.6 μm far-IR laser.

Keywords: laser machining, CO_2 laser, fused silica damage mitigation

*yang9@llnl.gov

1. INTRODUCTION

Mitigating damage growth on fused silica is important for extending the usable optics lifetime of fusion class laser systems. A small damage site on the surface of fused silica, once initiated, can quickly grow in size when exposed to additional laser shots[1]. To arrest the damage growth, two laser-based mitigation approaches have been investigated at Lawrence Livermore National Laboratory (LLNL); these techniques are referred to here as the non-evaporative and evaporative approaches[2,3]. In the non-evaporative approach, the laser is operated at moderate power with large beam size and long exposure time to heat silica above the glass transition point, but well below the evaporative limit, so as to melt and re-flow the damaged glass surface. In the evaporative approach, short pulse, high peak power CO_2 laser is focused to a small spot size and raster-scanned over the damage site using galvanometer mirrors so as to evaporate away the damage volume.

Both mitigation approaches have so far used far-infrared (IR) 10.6 μm CO_2 laser because of the close match between 10.6 μm laser wavelength and the silica absorption peak. Silica's high absorption at 10.6 μm, however, limits CO_2 laser penetration into the bulk and prevents healing of deep damage sites. As a result, the non-evaporative mitigation approach is currently limited to repairing small (<100 μm diameter) and shallow (<30 μm deep) damage sites. It has been suggested that larger and deeper damage sites can be mitigated by using a laser with a wavelength that is less absorbing in silica. For example, silica's absorption in the mid-IR (4-5 μm range) is two orders of magnitude lower relative to that at 10.6 μm, which is low enough to permit deep heat penetration, while still high enough for effective light absorption[4]. Recently, demonstration of the deep crack healing using a custom-built mid-infrared laser operating at 4.6 μm was carried out in our laboratory[5]. Although this initial work clearly demonstrated the potential of using mid-IR 4.6 μm lasers for mitigating deep damage sites, the relative merit of mid-IR (4.6 μm) versus far-IR (10.6 μm) lasers for damage growth mitigation was not quantified and the parameter space where 4.6 μm laser is advantageous relative to 10.6 μm lasers for deep crack healing was not clarified. The present study was carried out to answer these questions. The paper is divided into the following sections: in section 2, we will present our experimental setup and discuss measurement of temperature-dependent silica absorption coefficient, $\alpha(T)$, at 4.6 μm. In section 3, we will use the measured $\alpha(T)$ at 4.6 μm to derive a temperature distribution model for 4.6 μm laser-heated silica. Based on the

temperature distribution models, we will compare the heat penetration depths when mid-IR and far-IR lasers are used to heal deep damage cracks under minimum-evaporative heating. A relationship is then found which relates heat penetration to depth where effective crack healing can occur. Finally, a figure-of-merit (FOM) is defined to quantify the efficiency of mitigating deep damage sites using the two lasers.

2. EXPERIMENTAL

2.1 Experimental setup

The experimental setup is shown in Fig. 1. The 4.6 μm laser used in this study is a frequency-doubled Q-switched 9.2 μm CO_2 laser (Coherent DEOS MID-IR-2). The laser has a pulse repetition rate of 75 kHz, with a pulse width of 22 ns and a maximum average power of 6 watts. The high pulse repetition rate implies that the laser output can be considered quasi-continuous-wave for the present application. To vary the power incident on the sample, a variable attenuator is used. In our experimental setup, the output of the laser is first collimated and then focused onto the fused silica sample using un-coated CaF_2 lenses. The beam diameter at the sample is varied by changing the beam size incident on the final focusing lens. For monitoring the laser-heated silica surface temperature in-situ, an infrared radiometer, consisting of a liquid-nitrogen cooled HgCdTe focal plane array with a band-pass cold filter, is used to detect black body emission in a narrow band centered on 8.9 μm. A microscope setup, attached with a CCD camera, is used to view the sample during heating.

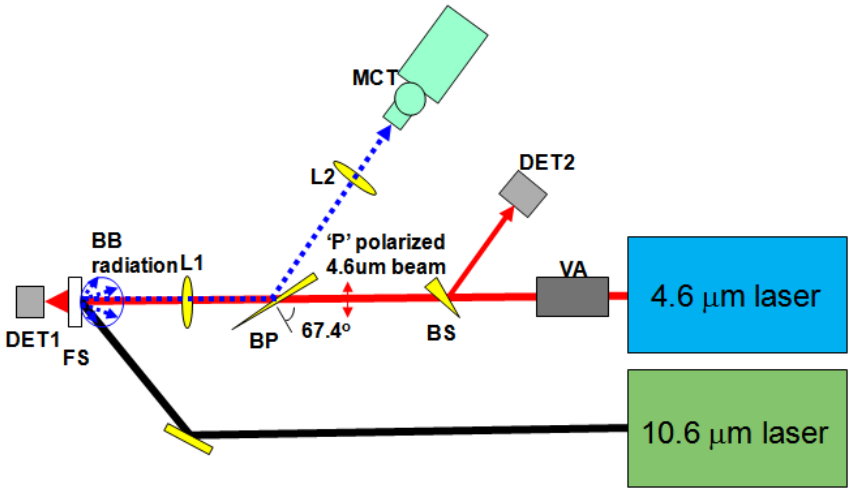

Figure 1. Experimental layout for 4.6 μm laser heating of fused silica and measurement of silica's $\alpha(T)$ at 4.6 μm, 10.6 μm laser is used for heating a thin fused silica sample for absorption coefficient measurement as described in the text. Symbols used in the figure are: VA (variable attenuator), DET1&2 (HgCdTe detectors), BS (beam splitters), BP (ZnSe wedge oriented at Brewster's angle), L1&L2 (lenses) and MCT (HgCdTe focal plane array)

2.2 Measurement of fused silica's $\alpha(T)$ at 4.6 μm

To accurately predict the temperature distribution inside fused silica when heated with the 4.6 μm laser, it is necessary to know the temperature dependence of absorption coefficient $\alpha(T)$. Since no $\alpha(T)$ data at 4.6 μm for silica is available in the literature, we proceeded to measure $\alpha(T)$ in our laboratory over the temperature range of interest. The measurement is performed by detecting the 4.6 μm transmission through a thin (120±1 μm) fused silica plate when it is heated to various temperatures. For heating the silica plate, a 10.6 μm laser (Synrad firestar V20) is incident on the silica sample with the heating spot centered on the 4.6 μm beam and with an elliptical beam size (7.9 mm×4.8 mm $1/e^2$ beam diameters) that is more than 10× the size of the 4.6 μm beam. Since the heating beam is significantly over-sized relative to the 4.6 μm beam, heat flow within the 4.6 μm beam region is essentially 1-D. In the steady-state, the 1-D heat diffusion is expected to result in a uniform axial temperature distribution within the thin slab. Thus, by using an over-sized heating beam and by waiting 60 seconds after turn-on of the heating beam before making the measurements, we ensured uniform radial and axial temperature profiles within the region traversed by the 4.6 μm beam. For measuring the

temperature of the heated region, the infrared radiometric setup is used. Both the incident and transmitted 4.6 μm laser powers are monitored using separate thermo-electrically cooled HgCdTe detectors (VIGO PVMI-2TE).

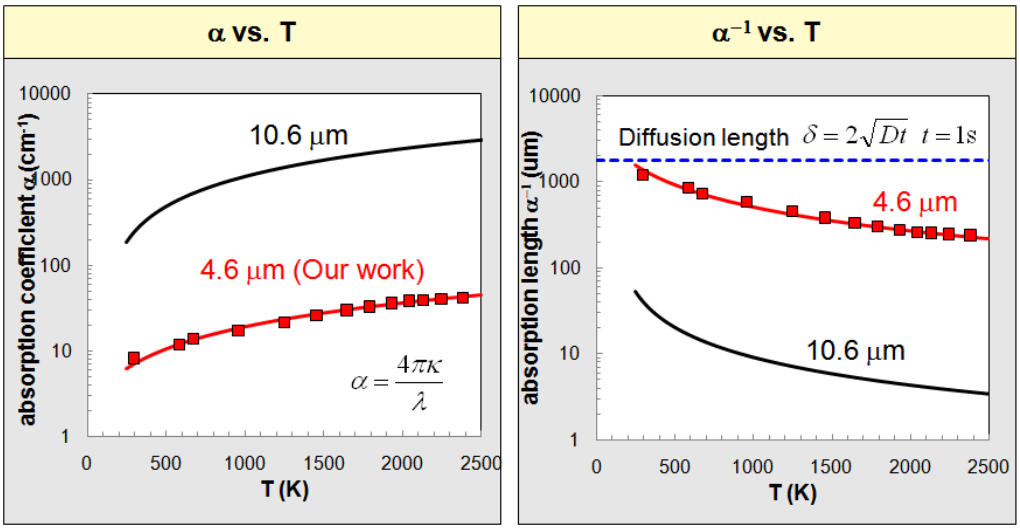

a) b)

Figure 2 Measured absorption coefficient $\alpha(T)$ a) and absorption length α^{-1} b) plotted versus silica temperature. Symbols are data while solid lines are best fits. Also plotted is the 10.6 μm data from Mclachlan et al[6].

The measured 4.6 μm transmission through the thin silica plate drop from 90% to 60% when the plate temperature is heated between room temperature and 2300K.. Taking into account the multiple reflections in a plane-parallel plate with internal loss, the extinction coefficient κ and the absorption coefficient $\alpha=4\pi\kappa/\lambda$ can be calculated. Fig. 2 displays the extracted silica absorption coefficient (α) and absorption length (α^{-1}) at 4.6 μm plotted versus temperature. Also included in the plot is the silica absorption data at 10.6 μm from Mclachlan et al[6]. As shown in Fig. 2, although $\alpha(T)$ increases with temperature at both wavelengths, the magnitude of $\alpha(T)$ at 4.6 μm is two orders of magnitude lower relative to 10.6 μm absorption. The lower absorption coefficient at 4.6 μm translates into a much longer absorption length as shown in Fig. 2b). Compared with silica thermal diffusion length, $\delta = 2\sqrt{Dt}$, of 1.8 mm assuming a 1 second long exposure, the 10.6 μm absorption length is much shallower, which means that 10.6 μm laser heating of silica can be approximated as surface heating. The same approximation cannot be made for the 4.6 μm heating case, however, since 4.6 μm absorption length is comparable to thermal diffusion length. In this case, heating is volumetric in nature. The implications for this difference in α will be discussed in the next section.

3. RESULTS AND DISCUSSION

3.1 Silica temperature distribution model due to 4.6 μm laser heating

Owing to silica's large absorption at 10.6 μm, heating of silica by 10.6 μm lasers occurs essentially at the surface. This conclusion was corroborated by our previous study[7], where peak surface temperature of silica was measured as a function of incident 10.6 μm laser power. As shown in Fig. 3a), measured silica surface temperature rises up linearly versus power which agrees well with solution of heat-flow equation assuming surface heating and using effective thermal parameters that are independent of temperature. In contrast, when silica is heated with 4.6 μm lasers, silica surface temperature increases super-linearly as shown in Fig. 3b). The nonlinear temperature rise is not accounted for using the 10.6 μm temperature distribution model, which predicts linear temperature rise strictly. By assuming different absorption coefficients in the 10.6 μm temperature distribution model, however, model prediction can be made to overlap a different portion of the 4.6 μm data. This suggests to us that silica's temperature varying absorption coefficient at 4.6 μm needs to be taken into account in order to explain the super-linear temperature rise when silica is heated with the mid-IR laser. Unfortunately, inclusion of α as a function of temperature in the heat flow equation necessitates

solving the full nonlinear heat equation. Following the approach of Mansuripur[8], the nonlinear heat-flow equation was solved numerically using the Finite-Difference-Time-Domain (FDTD) technique, using the same effective thermal parameters as in the 10.6 μm case, but including the measured 4.6 μm $\alpha(T)$. As shown in Fig 3b), solution of the nonlinear heat flow equation, with $\alpha(T)$ included, agrees well with the measured super-linear peak surface temperature rise. Good agreement is also obtained between numerical calculation and measured radial and temporal temperature profiles (not shown here). The good agreement between data and calculation validates our assumption that the nonlinear surface temperature rise in the 4.6 μm laser heating case arises from a positive feedback effect caused by the temperature varying absorption coefficient: as silica is heated by 4.6 μm laser irradiation, α in the heated region increases which in turn results in more heat being absorbed within the heated region, and thus accelerating temperature rise.

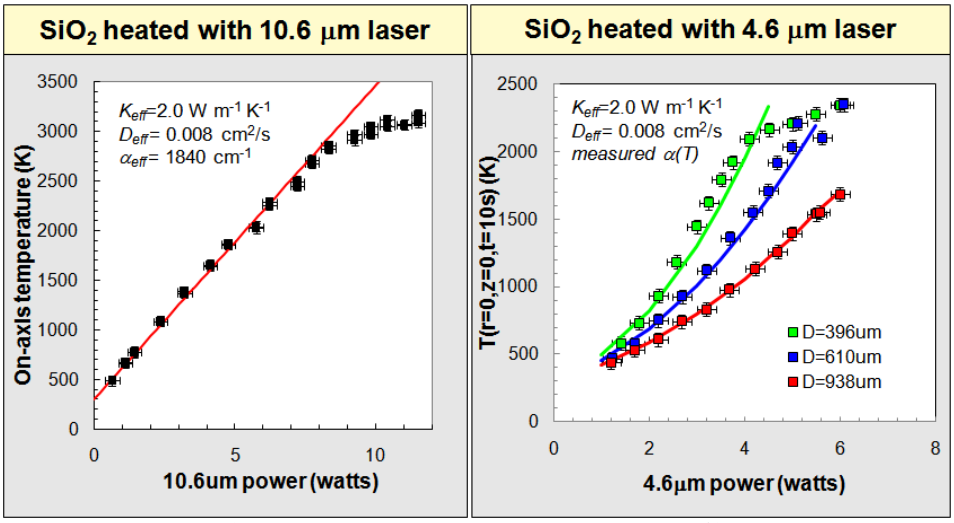

a) b)

Figure 3. Silica peak surface temperature heated with a) 10.6 μm and b) 4.6 μm lasers. The symbols are measured peak surface temperature using infrared radiometry. Solid lines are calculated from temperature distribution models using thermal parameters as shown in the inset.

3.2 Comparison of heat penetration depths

Using the temperature distribution models derived, we compare the heat penetration depths in silica when the two lasers are used for damage mitigation following the non-evaporative approach. Fig. 4a) and b) show the calculated 2D temperature contours at the end of a 10 seconds long constant power laser exposure, and assuming 1 mm ($1/e^2$) beam diameter, and with laser powers chosen to achieve peak surface temperature of 2000K at beam center. Since the silica absorption coefficient is lower at 4.6 μm, it requires 7.6W of 4.6 μm laser power to heat silica surface to 2000K versus 5.2W required for 10.6 μm laser heating. As shown by the widely spaced temperature contours in fig 4a), the decreased absorption at 4.6 μm allows heat to penetrate deeper into the silica bulk. In contrast, the contour lines in the 10.6 μm heating case are much more closely spaced together near the surface, suggesting localized heating near the surface and steep temperature gradients. For the calculation shown, the axial temperature drops from 2000 K 1700 k within 50 μm of the surface in the 10.6 μm case, while the same temperature drop does not occur until 280 μm below the surface when heated with 4.6 μm laser.

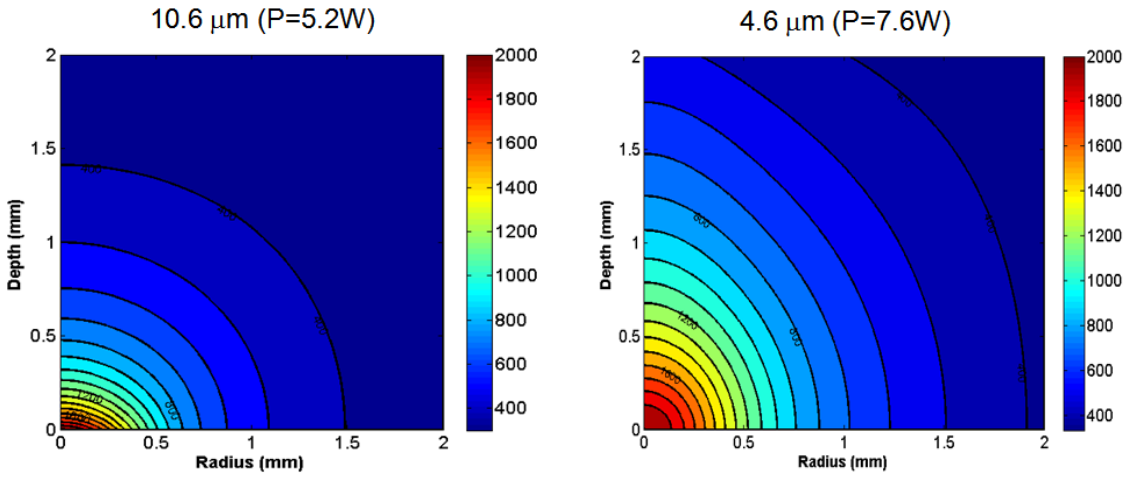

a) b)

Fig. 4 Calculated 2D temperature contour plots of silica when heated with a) 10.6 μm lasers and b) 4.6 μm lasers. The center of the laser beam is at r=0 and z=0. Contour lines are spaced apart by 100 K.

3.3 Effective crack healing depth

Deeper heat penetration is expected to result in healing of deep cracks. Crack healing occurs when the glass is heated to above glass transition point so as to allow surface tension driven viscous flow to fill-in the cracks[9]. The rate at which capillary-driven glass flow evolves is given by the time constant

$$\tau = \frac{\eta(T)w}{\pi\sigma},$$

Where $\eta(T)$ is silica's viscosity, w is the crack width, and σ is the surface tension. For silica, viscosity is highly temperature dependent[10], while surface tension is nearly constant at 300 dynes/cm[11]. Assuming a crack width w of 1 μm, the time constant, τ, varies from over an hour to tens of seconds when the glass is heated to between 1600 and 1800 K. In our non-evaporative mitigation approach, the damage site is irradiated with minutes-long exposure to maintain reasonable throughput. Therefore, we conclude from this analysis that healing of cracks with width of 1 μm or less can occur down to the depth where silica is heated to at least 1700 K under the non-evaporative mitigation conditions.

3.4 Figure of merit for healing deep cracks

Based on the discussion from the previous section, we can define an effective crack healing depth, z_{eff}, as the glass depth where the steady state temperature reaches 1700 K. Additionally, if we further impose the non-evaporative condition that the peak surface temperature is at 2000 K, and define the power required to reach this temperature as P_0, we arrive at a figure-of-merit that quantifies the crack healing efficiency as

$$F.O.M. = \frac{z_{eff}}{P_o}.$$

According to the *FOM* defined here, *FOM* is higher when z_{eff} increases for a fixed P_0 or when P_0 decreases for a given z_{eff}.

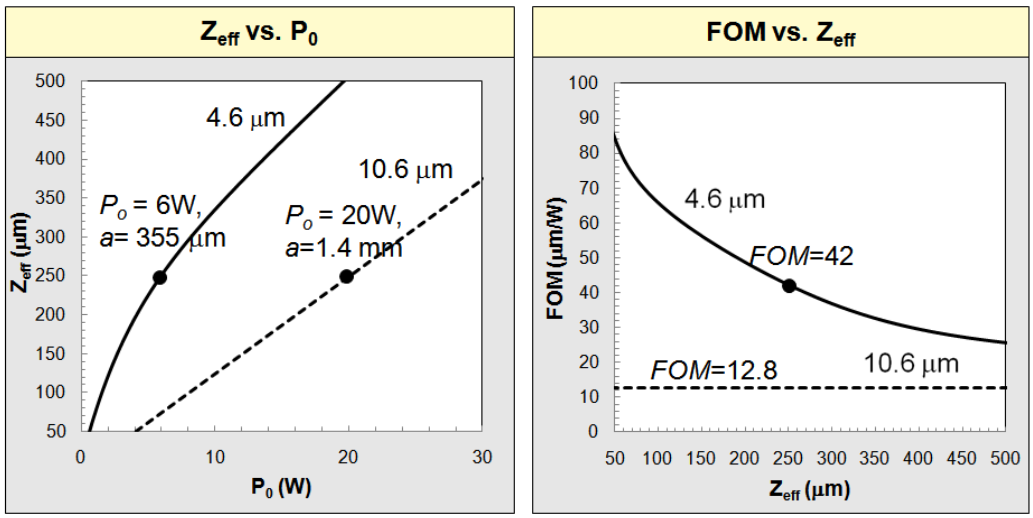

a) b)

Figure 5. a) Calculated z_{eff} versus P_0 for 4.6 μm and 10.6 μm heated silica, and b) FOM for the two laser cases plotted versus z_{eff}.

Using the temperature distribution models for the two laser-heating cases, we've calculated z_{eff} and P_0 and the results are shown in Fig. 5a). For a given P_0, the beam radius a that will yield a peak surface temperature of 2000K is first determined. The effective crack healing depth, z_{eff}, for the given P_0 and a_0 is then calculated from the temperature distribution models. In the case of 10.6 μm heating, z_{eff} increases linearly with P_0 with a slope of 12.8 μm/W. At all power levels considered, z_{eff} is deeper when silica is irradiated with 4.6 μm laser as opposed to 10.6 μm laser. Equivalently, at a fixed z_{eff} within the 500 μm range considered, less power is required to achieve a fixed z_{eff} when a 4.6 μm laser is used versus when a 10.6 μm laser is applied. For example, to achieve a z_{eff} of 250 μm using a 4.6 μm laser would only require a power of 6 W focused to a 1/e beam radius of a=355 μm. In contrast, to achieve the same z_{eff} using a 10.6 μm laser would require as much as 20 W of power spread out over a radius of 1.4 mm.

The increased efficiency is reflected in the higher *FOM* as shown in Fig. 5b). For z_{eff} up to 500 μm, *FOM* for 4.6 μm laser is consistently higher than that for 10.6 μm laser. In particular, at z_{eff} of 250 μm, FOM is 3.3× higher (42 μm/W versus 12.8 μm/W) when a 4.6 μm laser is used versus when a 10.6 μm laser is used. At large z_{eff} , however, *FOM* for the 4.6 μm laser is seen to approach FOM of 10.6 μm laser. The decline of 4.6 μm *FOM* can be attributed to the increase in beam radius a that is required to achieve deeper z_{eff} such that in the limit of large z_{eff} the surface heating condition, $a>>\alpha^{-1}$, is approached and any further increase in 4.6μm power produces a linear increase in z_{eff} as in the 10.6 μm case. Nonetheless, for crack healing to depths of at least 500 μm, the laser heating will be more efficient and the treatment can remain well-localized using a 4.6 μm laser as compared to a 10.6 μm laser.

4. CONCLUSION

To summarize, in this study, we have quantified the relative advantage of using 4.6 μm lasers versus 10.6 μm lasers for mitigating deep damage sites under minimum evaporative condition. We started out by deriving a temperature distribution models for laser-heated-silica using the two lasers. We find that, in contrast to the 10.6 μm laser heating case where temperature distribution is well described by analytical solution to the linear heat-flow equation assuming surface heating and using constant effective thermal parameters, temperature distribution in the 4.6 μm laser heating case can only be obtained by numerically solving the full nonlinear heat-flow equation taking into account the temperature varying silica absorption at 4.6 μm. Using the temperature models derived, we then compared the heat penetration expected using the two lasers for damage growth mitigation following the non-evaporative approach. The deeper heat penetration possible using the 4.6 μm laser is next shown to lead to healing of deeper cracks. Defining an effective crack

healing depth, we arrive at a figure of merit for deep crack healing that finally permitted us to quantify the relative advantage of 4.6 μm lasers versus 10.6 μm lasers for mitigating deep damages.

The authors would like to acknowledge Dr. Michael Feit, Dr. James Stolken, Ryan Vignes, and Dr. Isaac Bass for stimulating discussions relating to numerical solution of the heat equation. This work was performed under the auspices of the U.S. Department of Energy by Lawrence Livermore National Laboratory under contract DE-AC52-07NA27344.

REFERENCE

[1] M. A. Norton, L. W. Hrubesh, W. Zhouling, E. E. Donohue, M. D. Feit, M. R. Kozlowski, D. Milam, K. P. Neeb, W. A. Molander, A. M. Rubenchik, W. D. Sell, and P. Wegner, "Growth of laser initiated damage in fused silica at 351 nm," Proc. SPIE **4347**, 468 (2001).

[2] J. Adams, J.D. Bude, M. Bolourchi, G.M. Guss, M.J. Matthews, M.C. Nostrand, "Results of applying a non-evaporative mitigation technique to laser-initiated surface damage on fused silica," Proc. SPIE **7842**, 81 (2010).

[3] I.L. Bass, G.M. Guss, M.C. Nostrand, P.J. Wegner, "An improved method of mitigating laser-induced surface damage growth in fused silica using a rastered, pulsed CO_2 laser," Proc. SPIE **7842**, 78 (2010).

[4] R. Kitamura, L. Pilon, and M. Jonasz, "Optical constants of silica glass from extreme ultraviolet to far infrared at near room temperature," Appl. Opt. **46**, 8118-8133 (2007).

[5] G. Guss, I. Bass, V. Draggoo, R. Hackel, S. Payne, M. Lancaster, and P. Mak, "Mitigation of growth of laser initiated surface damage in fused silica using a 4.6-micron wavelength laser," Proc. SPIE **6403**, 64012 (2006).

[6] A. D. McLachlan and F. P. Meyer, "Temperature dependence of the extinction coefficient of fused-silica for CO_2-laser wavelengths," Appl. Opt. **26**, 1728-1731 (1987).

[7] S. T. Yang, M. J. Matthews, and S. Elhadj, "Thermal transport in CO_2 laser irradiated fused silica: in situ measurements and analysis " J. of Appl. Phys. **106**, 1031061-1031067 (2009).

[8] M. Mansuripur, G. A. N. Connell, and J. W. Goodman, "Laser-induced local heating of multilayers," Appl. Opt. **21**, 1106-1114 (1982).

[9] M. D. Feit and A. M. Rubenchik, "Mechanisms Of CO_2 laser mitigation of laser damage growth in fused silica," Proc. SPIE, **4932**, 91-102 (2002).

[10] R. H. Doremus, "Viscosity of silica," J. Appl. Phys. **92**, 7619-7629 (2002).

[11] N. M. Parikh, "Effect of Atmosphere on Surface Tension of Glass," J. of American Ceramic Society **41**, 4 (1958).